A reactive potential for hydrocarbons with intermolecular interactions

Steven J. Stuart, Alan B. Tutein, and Judith A. Harrison

Citation: The Journal of Chemical Physics **112**, 6472 (2000); doi: 10.1063/1.481208
View online: http://dx.doi.org/10.1063/1.481208
View Table of Contents: http://aip.scitation.org/toc/jcp/112/14
Published by the American Institute of Physics

A reactive potential for hydrocarbons with intermolecular interactions

Steven J. Stuart[a)]
Department of Chemistry, Clemson University, Clemson, South Carolina 29634

Alan B. Tutein[b)] and Judith A. Harrison[c)]
Department of Chemistry, U.S. Naval Academy, Annapolis, Maryland 21402

(Received 7 May 1999; accepted 19 January 2000)

A potential function is presented that can be used to model both chemical reactions and intermolecular interactions in condensed-phase hydrocarbon systems such as liquids, graphite, and polymers. This potential is derived from a well-known dissociable hydrocarbon force field, the reactive empirical bond-order potential. The extensions include an adaptive treatment of the nonbonded and dihedral-angle interactions, which still allows for covalent bonding interactions. Torsional potentials are introduced via a novel interaction potential that does not require a fixed hybridization state. The resulting model is intended as a first step towards a transferable, empirical potential capable of simulating chemical reactions in a variety of environments. The current implementation has been validated against structural and energetic properties of both gaseous and liquid hydrocarbons, and is expected to prove useful in simulations of hydrocarbon liquids, thin films, and other saturated hydrocarbon systems. © *2000 American Institute of Physics.* [S0021-9606(00)50814-9]

I. INTRODUCTION

Computational chemists have long made use of classical molecular simulations, including molecular dynamics and Monte Carlo methods, to study systems of chemical interest. However, most of the potential functions used in these simulations are intended for modeling physical processes, not chemical reactions. Most of these simulation techniques simulate physical processes, and not chemical reactions. The formation and breaking of chemical bonds are inherently quantum mechanical processes, and are often studied using first-principles methods. Nevertheless, classical potentials do exist that can empirically model changes in covalent bonding.

One successful method for treating covalent bonding interactions in computer simulations is the Tersoff-type potential.[1,2] Unlike traditional molecular mechanics force fields,[3–10] the Tersoff model allows for the formation and dissociation of covalent chemical bonds during a simulation. Many-body terms reflecting the local coordination environment of each atom are used to modify the strength of more conventional pairwise terms. With this approach, individual atoms are not constrained to remain attached to specific neighbors, or to maintain a particular hybridization state or coordination number. Models of this sort, despite being purely classical, can provide a realistic description of covalent bonding processes in nonelectrostatic systems. Potentials of this type have been developed to treat systems containing silicon,[1] carbon,[11,12] germanium,[2] oxygen,[12] or hydrogen,[12] as well as heterogeneous systems containing various combinations of these species.[2,13–16]

One particularly successful example of a Tersoff potential is the reactive empirical bond-order (REBO) potential developed by Brenner.[15–18] This model uses a Tersoff-style potential to describe the covalent bonding interactions in carbon and hydrocarbon systems. Originally developed for use in simulating the chemical vapor deposition of diamond,[15] the REBO potential has recently been extended to provide more accurate treatment of the energetic, elastic, and vibrational properties of solid carbon and small hydrocarbons.[18] In various incarnations, this potential has been used to model many different materials and processes, including fullerenes,[17] carbon nanotubes,[19] amorphous carbon,[20] and the tribology and tribochemistry of diamond interfaces.[21–27]

The REBO potential is not appropriate for studying every hydrocarbon system, however. In particular, the absence of dispersion and nonbonded repulsion terms makes the potential poorly suited for any system with significant intermolecular interactions. This is the case for many important hydrocarbon systems, including liquids and thin films, as well as some solid-state materials such as graphite and fullerenes. Even covalent materials such as diamond can benefit from a treatment including nonbonded interactions. The bulk phase is dominated by covalent interactions, but longer-range forces become quite important when studying interfacial systems.[28]

Various attempts have been made previously to combine nonbonded interactions with the Tersoff or REBO potentials in a way that preserves the reactive capabilities of the model.[29–31] One way to do this is to simply reduce the repulsive barrier associated with the Lennard-Jones or other potential,[32] although this results in barriers which are too large for radical species and too small for saturated compounds. Another alternative, taken by Nyden *et al.*,[30] is to allow bonds to dissociate with a Morse potential, and explic-

[a)]Electronic mail: ss@clemson.edu
[b)]Electronic mail: tutein@nadn.navy.mil
[c)]Electronic mail: jah@nadn.navy.mil

itly check for recombination reactions between dissociated radicals. This approach has been used to model thermal decomposition of polymers,[30] but is not general enough to treat arbitrary reactions in hydrocarbons, such as addition across unsaturated bonds. Another method, used by Che *et al.*,[31] is to reduce the repulsive nonbonded interactions based on the covalent interaction energy, rather than the distance. This method can help eliminate nonbonded interactions during bond dissocations, but will again tend to overestimate barriers in association reactions.

In addition to lacking nonbonded interactons, the REBO potential also lacks a torsional potential for hindered rotation about single bonds. This has not prevented the potential from being used to model small hydrocarbons or functional groups in the past.[24,33] However, an accurate representation of torsional interactions should allow these systems to be treated with greater accuracy, and will also permit the study of larger hydrocarbons.

A potential is presented here that addresses these shortcomings in the REBO potential, in ways that improve upon earlier extensions to the REBO model. This new potential has been developed for use in simulating reactivity in condensed-phase systems where the REBO potential cannot be used, and can in principle be used for arbitrary hydrocarbon systems. But the primary goal was to make progress towards a fully reactive intermolecular potential, rather than to supplant the many existing potentials for modeling nonreactive hydrocarbons.

Section II reviews the REBO potential and details the modifications that were required to introduce nonbonded and torsional interactions. The fitting procedure used to parametrize the new potential is described in Sec. III. Section IV discusses the structural and energetic properties that are obtained when the new model is applied to a variety of carbon and hydrocarbon systems, and Sec. V summarizes the novel characteristics of the new potential and describes the situations in which it is expected to prove most useful. An appendix presents in compact form all of the equations necessary to describe the current model.

II. POTENTIAL

The potential described in this article is based on the reactive empirical bond-order potential of Brenner.[15–18] Because the new potential introduces nonbonded interactions through an adaptive treatment of the intermolecular interactions, it shall be referred to here as the adaptive intermolecular REBO potential (AIREBO). The new portions of the potential will be described below in detail. The covalent bonding contributions of the REBO potential are largely unchanged, and will be discussed only briefly. For a more exhaustive discussion of the development of the REBO potential, the reader is referred to the original authors.[15,17,18] For completeness, all of the equations and parameters necessary to fully implement the current model—including those that are unchanged from the REBO model—are compiled in the appendix.

As originally developed, the REBO potential is exclusively short-ranged. Two atoms interact directly only if they are separated by a distance less than a covalent-bonding cutoff of $r_{ij}^{\max}$ (e.g., 2.0 Å for C–C bonds).

Each pair of covalently bonded atoms interacts via a potential,

$$E_{ij}^{\mathrm{REBO}} = V_{ij}^{R}(r_{ij}) + b_{ij} V_{ij}^{A}(r_{ij}), \tag{1}$$

where V_{ij}^{R} and V_{ij}^{A} are repulsive and attractive pairwise potentials determined by the atom types (carbon or hydrogen) of atoms i and j, and that depend only on the distance r_{ij} between the two atoms. Through its dependence on the many-body term b_{ij}, however, the value of E_{ij}^{REBO} also depends on the position and chemical identity of atoms close to the $i-j$ bond.

The b_{ij} bond-order term is the hallmark of a Tersoff-type potential. A variety of chemical effects that affect the strength of the covalent bonding interaction are all accounted for in this term. Coordination numbers, bond angles, and conjugation effects all contribute to the strength of a particular bonding interaction in the REBO potential. For example, the carbon–carbon b_{ij} term is larger between triply coordinated (sp^2) carbon atoms than between quadruply coordinated (sp^3) carbons. This weights the attractive term more heavily for sp^2 carbons, resulting in an increased strength for double bonds. It should be emphasized that, despite this effective treatment of hybridization, the REBO model includes no explicit quantum mechanics. All descriptions of conjugation or hybridization states are derived entirely from the system geometry; the simulations treat the electronic degrees of freedom in a purely empirical manner. A complete discussion of the various contributions to the b_{ij} term is deferred to the appendix. Additional details can also be found in prior discussions of the REBO potential.[15,17,18]

A. Intermolecular interaction potential

The REBO potential is very successful at describing *intramolecular* interactions in carbon and hydrocarbon materials.[15] Despite its many successes, however, the potential includes no mechanism for treating *intermolecular* interactions. These include the dispersion and short-range repulsion effects that give rise to many of the properties of liquids, polymers, and thin-film hydrocarbon materials. In the current potential, the dispersion and intermolecular repulsion interactions are modeled with a Lennard-Jones (LJ) 12–6 potential,

$$V_{ij}^{\mathrm{LJ}}(r_{ij}) = 4\epsilon_{ij}\left[\left(\frac{\sigma_{ij}}{r_{ij}}\right)^{12} - \left(\frac{\sigma_{ij}}{r_{ij}}\right)^{6}\right]. \tag{2}$$

Although the repulsive wall of the 12–6 LJ interaction is known to be too hard,[34] this potential was chosen over competing models such as an exp-6 potential due to its mathematical convenience, small number of adjustable parameters, and widespread use. The inaccuracies involved are expected to be quite small for most applications.

The presence of intermolecular interactions raises several difficulties in a reactive potential. Foremost among these is the barrier formed by the steep repulsive wall of the LJ term, preventing nonbonded atoms from approaching close enough to interact via the REBO potential. Clearly, the re-

pulsive interactions must be diminished in certain circumstances to preserve the reactivity that is the key feature of the REBO potential.

A simple distance-dependent switch on the LJ interaction has been used by other authors.[29] This approach was viewed to be inadequate, because it is incapable of accounting for variations in the chemical environment. For example, two hydrogen atoms at a particular separation may repel one another if they are covalently bound to different molecules, yet may feel an attraction at the same distance as free radicals. To preserve the reactive character of the potential, the chemical characteristics of the system must be considered in determining when to include or exclude the LJ interaction.

Three criteria were chosen to determine whether, and at what distance, to switch off the LJ interaction. This decision is made adaptively, depending on: (i) the distance separating the pair of atoms in question, (ii) the strength of any bonding interaction between them, and (iii) the network of bonds connecting them. In general, two atoms will feel a LJ repulsion at short distances only if they are not likely to form a chemical bond, and if they are not vicinal (1–4) neighbors in the same molecule. The complete mathematical expression for the LJ interaction between atoms i and j is given by

$$E_{ij}^{\mathrm{LJ}} = S(t_r(r_{ij}))S(t_b(b_{ij}^*))C_{ij}V_{ij}^{\mathrm{LJ}}(r_{ij}) + [1-S(t_r(r_{ij}))]C_{ij}V_{ij}^{\mathrm{LJ}}(r_{ij}), \tag{3}$$

where $S(t)$ is a universal switching function,

$$S(t) = \Theta(-t) + \Theta(t)\Theta(1-t)[1-t^2(3-2t)], \tag{4}$$

with $\Theta(t)$ representing the Heaviside step function. The switching function $S(t)$ is unity for $t<0$ and zero for $t>1$, switching smoothly between these two values at intermediate t with a cubic spline. The function and its first derivative are continuous at the endpoints of the switching region.

The distance between a pair of atoms affects the strength of their LJ interaction through the $S(t_r(r_{ij}))$ term in Eq. (3). The scaling function $t_r(r_{ij})$,

$$t_r(r_{ij}) = \frac{r_{ij} - r_{ij}^{\mathrm{LJ\,min}}}{r_{ij}^{\mathrm{LJ\,max}} - r_{ij}^{\mathrm{LJ\,min}}}, \tag{5}$$

is used to rescale the domain of the switching function $S(t)$. When r_{ij} is greater than $r_{ij}^{\mathrm{LJ\,max}}$, $S(t_r(r_{ij}))$ will be zero and the pair distance has no impact on the LJ interaction. When $r_{ij}<r_{ij}^{\mathrm{LJ\,max}}$, on the other hand, the first term in Eq. (3) is nonzero, and the LJ interactions are contingent on the values of the other two switching functions.

The switching region $[r_{ij}^{\mathrm{LJ\,min}}, r_{ij}^{\mathrm{LJ\,max}}]$ was chosen such that the minimum of the LJ potential well remains unperturbed from the unswitched interaction, and such that there is no artificial reaction barrier due to LJ repulsions at short distances when the LJ interactions are switched off. With these constraints, the switching region has its maximum width when $r_{ij}^{\mathrm{LJ\,min}} = \sigma_{ij}$ and $r_{ij}^{\mathrm{LJ\,max}} = 2^{1/6}\sigma_{ij}$. The choice of $r_{ij}^{\mathrm{LJ\,min}} = \sigma_{ij}$ also has the advantage of guaranteeing that the second derivative of the potential is continuous at $r^{\mathrm{LJ\,min}}$.

The second criterion that can affect the LJ interaction is a bonding switch represented by the $S(t_b(b_{ij}^*))$ term in Eq. (3). The scaling function $t_b(b_{ij})$,

$$t_b(b_{ij}) = \frac{b - b_{ij}^{\min}}{b_{ij}^{\max} - b_{ij}^{\min}}, \tag{6}$$

converts a REBO bond-order term b_{ij} to a range suitable for use in the cubic spline switching function $S(t)$. When the bond order is large, indicating that covalent bonding will occur between the two atoms in question, t_b is greater than one and the repulsive LJ interactions will not be present. For low values of the bond order, indicating that covalent bonding is not likely, the LJ interaction will be included to a variable degree depending on the value of b_{ij}. For sufficiently low values of b_{ij}, the LJ repulsion will be undiminished.

The b_{ij}^* term in Eq. (3) differs subtly from the term b_{ij} used in the REBO potential. The adaptive LJ interaction in Eq. (3) will typically be evaluated for pairs of atoms at *intermolecular* distances. Because this separation typically exceeds the covalent bonding distance $r_{ij}^{\max}$, the REBO term b_{ij} is not an accurate representation of the bond order between atoms i and j. Consequently, the bond-order term b_{ij}^* in the nonbonded portions of the AIREBO potential represents a *hypothetical* b_{ij} term that is evaluated at $r_{ij}^{\min}$,

$$b_{ij}^* = b_{ij}\big|_{r_{ij}=r_{ij}^{\min}}. \tag{7}$$

The distances from atoms i and j to each of their neighbors are assumed to remain unchanged when evaluating b_{ij}^*.

The discussion above justifies the distance and bond-order switches that are applied to the LJ interaction. The third criterion used in evaluating the contingent LJ potential is a connectivity switch, represented by C_{ij} in Eq. (3). Because the interactions between first neighbors (1–2) and second neighbors (1–3) are modeled very well by existing components of the REBO potential, all LJ interactions are excluded for atom pairs that constitute first or second neighbors. Similarly, the 1–4 interactions are left to the dihedral-angle potential described below. This disregard of LJ interactions for closely bound neighbors is comparable to similar restrictions in molecular mechanics potentials, which treat bond stretches, angle bends, and dihedral rotations separately from nonbonded interactions. Unlike molecular mechanics potentials, however, the reactive AIREBO potential allows the nonbonded interactions to be turned smoothly on or off as bonding configurations change.

The smooth transition from bonded to nonbonded interactions as a molecule dissociates is implemented using bond-weight terms $w_{ij}(r_{ij})$. The bond weight w_{ij} is a number between zero and one, that is used as an indication of the bonding between atoms i and j. This permits the identification of atom pairs as bonded ($w_{ij}=1$), nonbonded ($w_{ij}=0$), or partially dissociated ($0<w_{ij}<1$). It is implemented as a distance-based switching function that varies smoothly from one to zero over a covalent bonding region,

$$w_{ij}(r_{ij}) = S'(t_c(r_{ij})) \tag{8}$$

with

$$t_c(r_{ij}) = \frac{r_{ij} - r_{ij}^{\min}}{r_{ij}^{\max} - r_{ij}^{\min}}. \tag{9}$$

The switching function $S'(t)$ is similar to the cubic spline function $S(t)$, but is implemented as a cosine-based switch for compatibility with the original REBO potential,

$$S'(t)=\Theta(-t)+\Theta(t)\Theta(1-t)\frac{1}{2}[1+\cos(\pi t)]. \tag{10}$$

Lennard-Jones interactions are disabled for any atom pair that is connected by a series of three or fewer bonds, and partially disabled if the connection is via a series of partially dissociated bonds. This is implemented using the C_{ij} connectivity switch in Eq. 3, defined using the strongest series of three or fewer bonds connecting i and j,

$$C_{ij}=1-\max\{w_{ij}(r_{ij}),w_{ik}(r_{ik})w_{kj}(r_{kj}),\forall k \\ w_{ik}(r_{ik})w_{kl}(r_{kl})w_{lj}(r_{lj}),\forall k,l\}. \tag{11}$$

When atoms i and j are neighbors, or are connected by one or two intermediate neighbors, C_{ij} is zero and there is no LJ interaction between the atoms. Thus the three criteria that affect the strength of the LJ interactions are distance, bond order, and connectivity. Reviewing the terms in Eq. (3) reveals that for the LJ interactions to be fully included, the atom pair in question must not be (1,4) neighbors, and must either be beyond a cutoff distance or have an unfavorable value of the bond order. Pairs that do not meet these criteria have LJ interactions which are partially diminished, or absent entirely.

B. Torsional interaction potential

The other new component of the AIREBO potential is a term dependent on dihedral angles. The original REBO potential lacked any torsional interactions about single bonds, reflecting its original focus on network solids such as diamond and small molecular fragments relevant to the chemical vapor deposition of diamond. With no barrier to rotation about single bonds, however, the original REBO potential is poorly suited for the simulation of saturated hydrocarbons larger than methane.

As with the nonbonded interactions, the reactive nature of the potential requires some modifications to the conventional method of introducing torsional interactions. The usual form[35] for the torsional potential is a cosine power series in the dihedral angle ω,

$$V=\frac{1}{2}\sum_{k=1}^{3}V_k[1-(-1)^k\cos(k\omega)]. \tag{12}$$

The coefficients V_k are chosen for each individual molecule based on the relative energies and barriers to rotation. But in a reactive potential, these energies and barriers must change as the molecule undergoes chemical reactions. Therefore, it is preferable if the symmetry of the torsional potential arises naturally from the local coordination environment, rather than being built into the parameter set.

This is accomplished in the current potential through the use of a torsional potential with a single minimum,

$$V^{\text{tors}}(\omega)=\epsilon\left[\frac{256}{405}\cos^{10}\left(\frac{\omega}{2}\right)-\frac{1}{10}\right]. \tag{13}$$

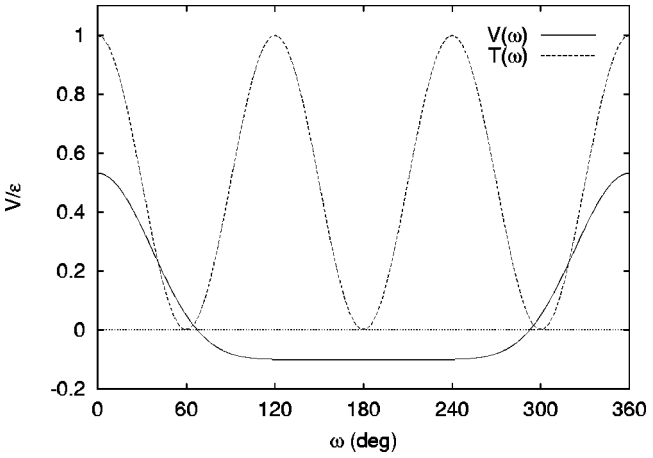

FIG. 1. Form of the atom-based dihedral-angle potential $V(\omega)$ and the resulting molecular torsional potential $T(\omega)$ for a single bond between sp^3-hybridized atoms with six identical substituents.

The constants in this equation are chosen such that when the torsional interactions are summed over the nine dihedral angles in a bond between identically substituted sp^3 carbons, the overall molecular torsional potential $T(\omega)$ has the expected threefold symmetry with a barrier height of ϵ:

$$T(\omega)=3V(\omega)+3V\left(\omega+\frac{2\pi}{3}\right)+3V\left(\omega-\frac{2\pi}{3}\right) \\ =\frac{1}{2}\epsilon[1+\cos(3\omega)]. \tag{14}$$

Figure 1 illustrates the form of the novel $V(\omega)$ torsional potential, as well as the $T(\omega)$ combined form.

This particular functional form for V^{tors} results in a torsional potential which is even about its single minimum and single maximum. These features reflect the physical symmetries of the repulsion (between atoms or bonds) that is assumed to be the fundamental origin of the torsional potential. These properties are shared by any even power of $\cos(\omega/2)$, i.e., $V(\omega)=\cos^{2n}(\omega/2)$. Equation (14) can only be recovered when $n=3$, 4, or 5. In the current work, the form corresponding to $n=5$ was chosen based on the relative size of the barriers in $V(\omega)$ and $T(\omega)$.

The torsional potential given by Eq. (13) is implemented in the AIREBO model for all dihedral angles in the system, in proportion to the bond weights that contribute to the dihedral angle,

$$E^{\text{tors}}=\frac{1}{2}\sum_i\sum_{j\neq i}\sum_{k\neq i,j}\sum_{l\neq i,j,k}w_{ij}(r_{ij})w_{jk}(r_{jk})w_{kl}(r_{kl}) \\ \times V^{\text{tors}}(\omega_{ijkl}). \tag{15}$$

The use of bond weights ensures that the torsional energy associated with a given dihedral angle will be removed smoothly as any of the consituent bonds are broken.

There is at least one other study that has attempted to implement torsional potentials in a Tersoff-type model.[36] In contrast to that work, the current model correctly predicts a barrier to rotation about homogeneously substituted sp^3–sp^3 bonds, and does not induce any angle-bending forces.

With the forms given above for the adaptive treatment of dispersion, intermolecular repulsion, and torsional interactions, the entire system energy is thus given by the expression

$$E = E^{\mathrm{REBO}} + E^{\mathrm{LJ}} + E^{\mathrm{tors}}, \tag{16}$$

with the various components of the energy given by the equations presented earlier and in the appendix.

This completes the description of the new potential model. The following section discusses a particular parametrization suitable for condensed-phase hydrocarbons. But the primary significance of the new model is that it extends the capabilities of current models. The methodology developed above is one of very few methods available for treating both chemical reactivity and intermolecular interactions within the same system using a simple, empirical potential.

III. FITTING PROCEDURE

Equation (16) describes a version of the REBO hydrocarbon potential with adaptive, intermolecular interactions. This framework could be used to introduce long-ranged interactions into any potential of the Tersoff type, without compromising the reactive character of the potential. As an illustration of the capabilities of the new model, it is parametrized here specifically for condensed-phase hydrocarbons. To fully define the potential, values must be given for each of the parameters in the model. This section will describe the fitting procedure used to obtain values for these parameters, for the current parametrization, and serves as an example for future development of similar models.

In parametrizing the hydrocarbon AIREBO potential model, it was decided to preserve the REBO parameters at their original values whenever possible. This was done for several reasons. First, there is a large community of workers currently using the REBO potential, and this strategy minimizes the amount of work required to upgrade the potential to include intermolecular effects. Second, the REBO potential provides an accurate description of covalent bonding in carbon and hydrocarbon materials. Although introducing LJ terms without modifying the REBO parameters does perturb the properties of the model somewhat, the effects are small in most systems where the REBO potential is applicable. Lennard-Jones interactions are typically on the order of 10^{-2} kcal/mol, whereas covalent bonding interactions are more typically 10^{2} kcal/mol. Because of this difference in energy scales between covalent and intermolecular interactions, the LJ contribution to the potential can be parametrized independently from the already well-parametrized REBO terms. Similarly, torsional interactions, typically contributing on the order of 1 kcal/mol, are small perturbations on the existing bonding terms, and can also be parametrized independently.

The parameters that specify the LJ interactions include σ_{ij} and ϵ_{ij}, where the atom types represented by i and j are either carbon and hydrogen. In addition, values must also be chosen for the switching function cutoffs $b_{ij}^{\max}$ and $b_{ij}^{\min}$. The $r_{ij}^{\mathrm{LJ\,min}}$ and $r_{ij}^{\mathrm{LJ\,max}}$ cutoffs are not independent parameters, but depend on the value of σ_{ij} as discussed below Eq. (5).

TABLE I. Switching function parameters in the AIREBO potential.

Switch	Value		Equation
	min	max	
r_{CC}	1.7	2.0	A6
r_{CH}	1.3	1.8	A6
r_{HH}	1.1	1.7	A6
N_{C}	3.2	3.7	A13
N	2	3	A16
s	0.1	0.1	A17
r'_{CC} (Å)	1.7	2.0	A20
r'_{CH} (Å)	1.3	1.6	A20
r'_{HH} (Å)	1.1	1.7	A20
$r_{\mathrm{CC}}^{\mathrm{LJ}}$ (Å)	σ_{CC}	$2^{1/6}\sigma_{\mathrm{CC}}$	A24
$r_{\mathrm{CH}}^{\mathrm{LJ}}$ (Å)	σ_{CH}	$2^{1/6}\sigma_{\mathrm{CH}}$	A24
$r_{\mathrm{HH}}^{\mathrm{LJ}}$ (Å)	σ_{HH}	$2^{1/6}\sigma_{\mathrm{HH}}$	A24
b_{CC}	0.77	0.81	A25
b_{CH}	0.75	0.90	A25
b_{HH}	0.32	0.42	A25

The values of these various parameters were chosen to optimize the fit to liquid-state hydrocarbon properties, while perturbing the properties of solid-state carbon polymorphs as little as possible. The procedure used to arrive at final parameter values was generally as follows. First, the values of $b_{ij}^{\min}$ and $b_{ij}^{\max}$ were chosen to guarantee that repulsive LJ interactions would only contribute between nonreactive species. By examining molecules in a variety of geometries, it was found that the modified bond order b_{CH}^{*} [see Eq. (7)] for a single hydrogen atom approaching a methane molecule never exceeded 0.75. A b_{CH}^{*} value of 0.75 or lower is thus an indication that no bond is likely to form between a given atom pair at closer distances. This is a system for which the repulsive interactions should always be present. Similarly, when a hydrogen atom approaches a methyl radical (a case for which the LJ repulsion should not be included), the value of b_{CH}^{*} is typically greater than 0.90. The values of $b_{\mathrm{CH}}^{\min}$ and $b_{\mathrm{CH}}^{\max}$ were thus chosen to be 0.75 and 0.90, respectively. The values of $b_{ij}^{\min}$ and $b_{ij}^{\max}$ for other combinations of atom types were chosen in a similar fashion. Their values appear in Table I. In general, the range between $b_{ij}^{\min}$ and $b_{ij}^{\max}$ was chosen to be as large as possible, while still allowing full LJ repulsion between unreactive species and negligible repulsion between radicals.

The properties of the AIREBO model depend only weakly on the exact width chosen for the $b_{ij}^{\min}$–$b_{ij}^{\max}$ switching range. Bond-order values in this range are typically only encountered when bonds are in the process of breaking or forming. Thus, the only system properties that depend critically on the values chosen are those related to the *dynamics* of bond dissociation or formation. While the energetics of covalent bonding are amenable to study by empirical potentials such as REBO and AIREBO, the dynamic aspects of bonding are inherently quantum mechanical, and are beyond the reach of these models.

In determining the LJ parameters σ_{ij} and ϵ_{ij}, only the homogeneous parameters ($i=j$) were taken to be independent parameters. The heterogeneous parameters σ_{ij} and ϵ_{ij} are determined using the usual Lorentz–Berthelot combining rules,[37]

TABLE II. Parameters for the AIREBO potential. All values except for ϵ_{ij}, σ_{ij}, and ϵ_{iCCj} are unchanged from the original REBO potential.[a]

Parameter	Value CC	Value CH	Value HH	Eqn.
Q_{ij} (Å)	0.313 460	0.340 776	0.370 471	A3
α_{ij} (Å^{-1})	4.746 5391	4.102 5498	3.536 2986	A3
A_{ij} (eV)	10 953.544	149.940 99	32.817 356	A3
$B_{ij}^{(1)}$ (eV)	12 388.792	32.355 187	29.632 593	A7
$B_{ij}^{(2)}$ (eV)	17.567 065	⋯	⋯	A7
$B_{ij}^{(3)}$ (eV)	30.714 932	⋯	⋯	A7
$\beta_{ij}^{(1)}$ (Å^{-1})	4.720 4523	1.434 4581	1.715 8922	A7
$\beta_{ij}^{(2)}$ (Å^{-1})	1.433 2132	⋯	⋯	A7
$\beta_{ij}^{(3)}$ (Å^{-1})	1.382 6913	⋯	⋯	A7
ρ_{ij} (Å)	⋯	1.09	0.7415 887	A14
ϵ_{ij} (eV)	0.002 84	$\sqrt{\epsilon_{CC}\epsilon_{HH}}$	0.001 50	A22
σ_{ij} (Å)	3.40	$\frac{1}{2}(\sigma_{CC}+\sigma_{HH})$	2.65	A22
ϵ_{iCCj} (eV)	0.3079	0.1787	0.1250	A28

[a]Reference 18.

$$\sigma_{ij}=\tfrac{1}{2}[\sigma_{ii}+\sigma_{jj}], \tag{17}$$

and

$$\epsilon_{ij}=\sqrt{\epsilon_{ii}\epsilon_{jj}}. \tag{18}$$

Thus four LJ parameters—σ_{CC}, σ_{HH}, ϵ_{CC}, and ϵ_{HH}—suffice to describe the intermolecular interactions.

Most potentials developed to describe condensed-phase hydrocarbons make use of significantly more than four LJ parameters. The parameters for a sp^3-hybridized carbon atom, for example, may differ from those of a sp^2 carbon. Molecular mechanics force fields carry this one step further, differentiating between different types of atoms based on the identity of neighboring atoms. While such an approach is possible with the model used here, it is less straightforward than in nonreactive models. Reactivity can change the bonding environment of a given atom, so an implementation of coordination-dependent LJ parameters must be done in a way that allows the parameters to vary smoothly as bonds are broken or formed. While certainly possible, such an approach was judged unnecessary for this initial implementation of the AIREBO model.

To determine the LJ parameters, a selection of properties of graphite and liquid hydrocarbons were chosen that depend critically on the nature of the intermolecular interactions. Because the interlayer interactions in graphite are decoupled almost completely from intralayer geometry changes, the interlayer separation of the graphite structure was taken as a convenient way to specify the σ_{CC} parameter. Similarly, once σ_{CC} was determined, the c_{33} elastic constant of graphite provided an unambiguous way of determining the ϵ_{CC} parameter.

After the carbon LJ parameters were obtained, the hydrogen LJ parameters were fit using the properties of liquid methane and liquid ethane. By adjusting the σ_{HH} and ϵ_{HH} parameters, it was possible to obtain accurate fits to the liquid structure of these two hydrocarbons and reasonable fits to their enthalpies of vaporization. The four LJ parameters that gave the best fit to this collection of experimental values are listed in Table II.

TABLE III. Structural, mechanical, and energetic properties of diamond. All REBO properties have been recalculated by the current authors.

Property	REBO	AIREBO	Experiment
r_{CC} (Å)	1.544	1.540	1.5445[a]
c_{11} (GPa)	1070[b]	1120(30)	1079(5)[c]
c_{12} (GPa)	120[b]	130(20)	124(5)[c]
c_{44} (GPa)	720[b]	770(20)	578(2)[c]
Bond energy (kcal/mol)	169.0	171.1	170[d]
$\Delta_f H_{298}$ (kcal/mol)	0.57	0.55	0.454[a]
Vacancy formation E (eV)	7.2	7.0	7.2[e]

[a]Reference 62.
[b]Reference 18 (and independently verified by the current authors).
[c]Reference 63.
[d]Reference 64.
[e]Reference 43.

The torsional potential described by Eq. (13) requires a barrier height ϵ to be specified for each of three different types of dihedral angles: H–C–C–H, C–C–C–H, and C–C–C–C. The value of ϵ_{HCCH} was determined by fitting to the experimental barrier of 2.9 kcal/mol for dihedral-angle rotation in ethane.[38] The values of ϵ_{CCCH} and ϵ_{CCCC} were chosen to reproduce the 3.4 kcal/mol torsional barrier in propane,[39] and the 0.90 kcal/mol energy difference between the *anti* and *gauche* forms of butane,[40] respectively. The resulting values of ϵ_{iCCj} are given in Table II.

IV. RESULTS

In characterizing the potential, we have chosen to compare the results to experiment, and to those produced by the REBO potential. There are certainly many other hydrocarbon potentials, many of which do an excellent job of predicting the physical properties of condensed-phase hydrocarbons.[3–10] In fact, most perform better than the current potential. But the AIREBO potential was developed with the aim of applying it in situations where reactivity is crucial. Thus it is important to compare the potential to another reactive potential, of which the REBO model is currently the most widely used.

A. Diamond and graphite

The properties of solid diamond as simulated by both REBO and AIREBO are summarized in Table III. For a network solid such as diamond, the dispersion forces acting between nonbonded atoms are universally attractive. When LJ interactions are included in the AIREBO model without modification of the REBO parameters, this causes a slight contraction in crystal lattice parameters. Consequently, the AIREBO model predicts an equilibrium C–C bond length for diamond that is shorter than the REBO and experimental values by 0.004 Å. The torsional potential does not affect the diamond structure, because all dihedral angles are either *gauche* or *anti*.

Elastic constants (obtained by finite difference at 298 K) are also slightly altered by the introduction of LJ interactions. At the equilibrium geometry, the increased compressive LJ forces are balanced by increased tensile covalent-bonding forces, leading to slightly stiffer force constants and slightly larger elastic constants. Because the elastic constants

TABLE IV. Structural, mechanical, and energetic properties of graphite.

Property	REBO	AIREBO	Experiment
r_{CC} (Å)	1.420	1.396	1.415[a]
r_l (Å)	···	3.354	3.354[a]
c_{11} (GPa)	1060[b]	1150	1060(20)[c]
c_{12} (GPa)	150[b]	150	180(20)[c]
c_{13} (GPa)	···	10	15(5)[c]
c_{33} (GPa)	···	40[d]	36.5(1.0)[c]
$\Delta_{sub}H_{298}$ (kcal/mol)	170.2	172.3	171.9[a]
$\Delta_f H_{298}$(rhomb) (kcal/mol)	0	0.0006	0.14(4)[a]
Vacancy formation E (eV)	7.5	7.7	7.6[e]

[a]Reference 62.
[b]The experimental r_l value was used in evaluating elastic constants for the REBO model.
[c]Reference 65.
[d]$c_{33}=40$ GPa at equilibrium geometry, 36 GPa at experimental geometry.
[e]Reference 44.

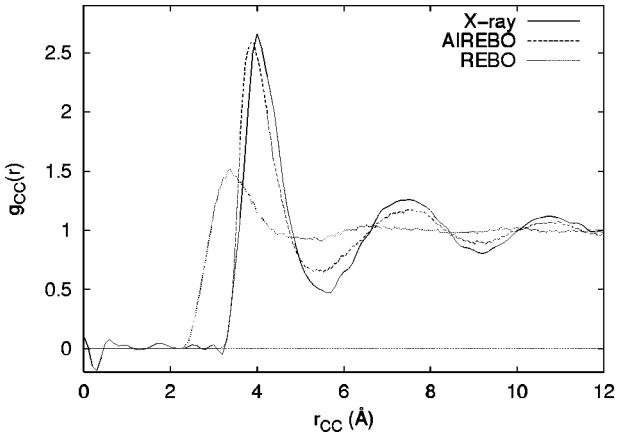

FIG. 2. Carbon–carbon pair correlation function $g_{CC}(r)$ for liquid methane at 92 K. Curves represent results from x-ray diffraction (Ref. 48), the AIREBO model, and the REBO model.

of diamond were used explicitly in fitting the parameters of the original REBO potential,[18] the agreement with experiment is slightly worse for AIREBO. The overall fit is still quite good.

Both potentials correctly indicate that diamond is slightly less stable than graphite, as indicated by the positive heats of formation. Both potentials also predict a bond energy (atomization energy) at 298 K that is within approximately 1 kcal/mol of the experimental value of 170 kcal/mol.

The properties of graphite, summarized in Table IV, demonstrate the same trends as were observed in diamond. The presence of attractive dispersion interactions shortens the C–C bonds, in this case by 0.02 Å. On the other hand, the LJ potential gives the AIREBO model the capability to model the interaction between the graphite layers, which was completely absent in the REBO potential model. The interlayer separation of $r_l=3.354$ Å was fit to the experimental value in determining the LJ parameters.

Once again, the elastic constants that depend on covalent bonding interactions are made somewhat stiffer by the introduction of LJ interactions. But elastic constants involving out-of-plane interactions now match experiment quite well. These elastic constants are undefined in the REBO model. Overall, both empirical potentials do quite well in reproducing the experimental elastic constants of diamond and graphite when compared to first-principles techniques.[41,42]

The sublimation enthalpy for graphite is near the experimental value of 171.9 kcal/mol for both models. In addition, the AIREBO model successfully predicts that the hexagonal form of graphite (ABAB stacking) is more stable than the rhombohedral form (ABCABC), although the energy difference is substantially smaller than that observed experimentally.

The central feature of the AIREBO model, as with the REBO model, is its ability to model chemical reactions in an empirical manner. Because the new terms describing dispersion, torsion, and intermolecular repulsion represent small corrections to the energy for the bulk solid phases that the REBO potential was designed for, the bonding energies remain largely unchanged. Several representative examples are listed in Tables III and IV. In addition to the bond energy quoted above, the vacancy formation energy in diamond is also given accurately by both models. This value is calculated to be 7.0 eV with the AIREBO model, slighty changed from the 7.2 eV predicted by the REBO model. The value predicted by density functional theory is also 7.2 eV.[43] (The vacancy formation energy differs from the bond energy of the solid because it takes into account the relaxation of the solid following vacancy formation.) For graphite, the vacancy formation energy is 7.7 eV under AIREBO, 7.5 eV under REBO, and 7.6 eV by density functional theory.[44]

B. Hydrocarbons

Although it does a respectable job of modeling extended solids such as diamond and graphite, the AIREBO potential was developed with molecular systems in mind. In particular, the goal was to obtain a potential that could be used for simulations of reactions in condensed-phase hydrocarbon systems, including liquids, polymers, and self-assembled monolayers. Consequently, the structural and energetic properties of several hydrocarbon liquids have been examined.

The liquid-state properties were all calculated using molecular dynamics simulations with 128 molecules, with LJ interactions terminated beyond 3σ. Appropriate long-range corrections were applied to the energy to account for the cutoffs.[45] The equations of motion were integrated with the velocity Verlet integrator and a simulation timestep of 0.5 fs. A generalized Langevin thermostat[46] was used to control the temperature. The pressure was maintained at 1 bar using a Berendsen-style barostat.[47]

One sensitive test of the dispersion and intermolecular repulsions is the pair correlation function of the liquid. The pair correlation functions $g_{CC}(r)$ for methane (at 92 K) and ethane (at 105 K and 181 K) that result from 100 ps of simulation are shown in Figs. 2 and 3. The structures of methane at 92 K and ethane at 181 K were used in fitting the AIREBO model parameters, and the model is able to reproduce the experimental pair correlation functions[48,49] quite accurately. The REBO model, on the other hand, generates liquids that are largely unstructured, with too many intermolecular pairs at close distances. This is due to the lack of

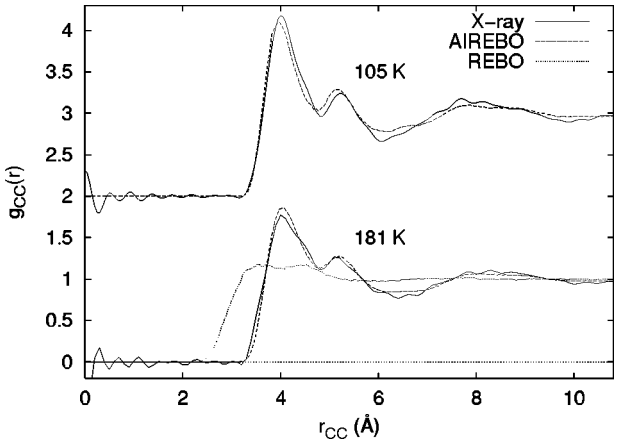

FIG. 3. Carbon–carbon pair correlation function $g_{CC}(r)$ for liquid ethane at 105 K (top) and 181 K (bottom). The 181 K results have been displaced by 2 units along the vertical. Curves represent results from x-ray diffraction (Ref. 49), the AIREBO model, and the REBO model.

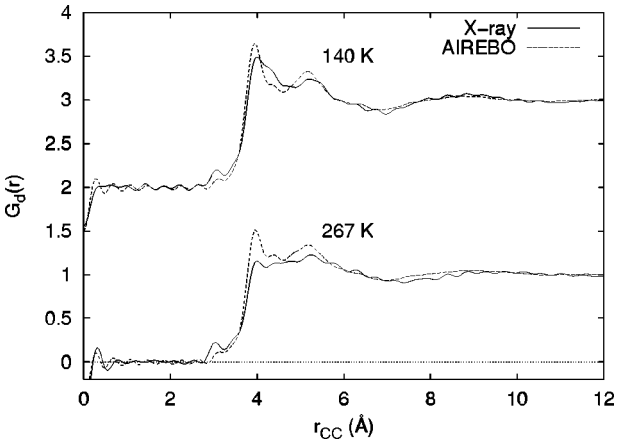

FIG. 5. Distinct intermolecular pair correlation function $G_d(r)$ for liquid butane at 140 K (top) and 267 K (bottom). The 267 K results have been displaced by 2 units along the vertical. Curves represent results from x-ray diffraction (Ref. 51) and the AIREBO model.

nonbonded interactions in the REBO potential, and was one of the prime motivations for the current work.

The structure of liquid ethane is correct not only at the 181 K temperature (near boiling) where the model was parametrized, but also at 105 K (near freezing), as shown in the upper curve of Fig. 3. This is an indication that the potential is transferable across a variety of conditions.

The structure of liquid alkanes not included in the fitting procedure is also well reproduced by the AIREBO model. Figures 4, 5, and 6 show the structure of propane, butane, and neopentane at various temperatures. Because each of these molecules contain nonequivalent carbon atoms, the experimental x-ray results[50–52] are reported as a combined pair correlation function G_d, which is not identical to the atom–atom pair correlation function g_{CC} that is usually calculated from simulation. The g_{CC} pair correlation functions calculated here have been converted to G_d functions for propane, butane, and neopentane, following Narten.[52] The difference between g_{CC} and G_d is small, but not insignificant, for butane and neopentane. Nonetheless, the $G_d(r)$ pair correlation functions may still be interpreted as a distribution of intermolecular C–C distances.

The structure of each of the alkanes is largely satisfactory. The peak locations are accurate, with the AIREBO model generating liquids that are slightly too structured at high temperatures. In propane (Fig. 4), the shoulder near 3.4 Å is absent in the simulation results. This peak indicates the presence of C–C pairs that are closer than the distance of closest intermolecular approach in each of the other hydrocarbon fluids studied, with the exception of benzene. The origin of this peak is not discussed in the experimental study, but is thought to be an artifact.[53]

For liquid butane (Fig. 5), the C1–C4 intramolecular separations are included in the $G_d(r)$ curve, as in the experimental data analysis.[51] The *gauche* conformer is responsible for the peak near 3.1 Å, while the *anti* conformer gives separations near 4.0 Å, coincident with the closest intermolecular interactions. The AIREBO model predicts a smaller peak at

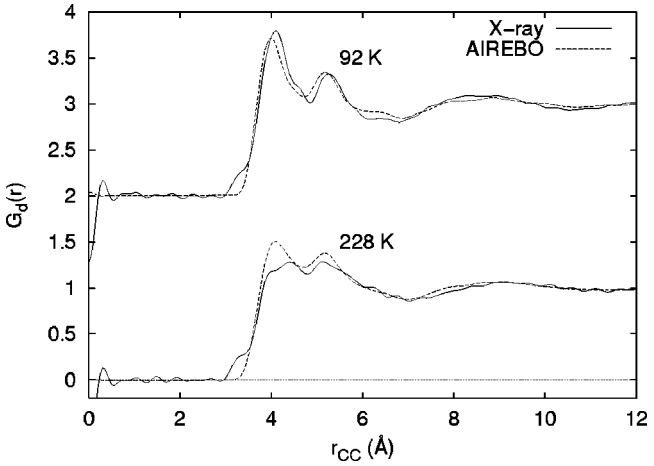

FIG. 4. Distinct intermolecular pair correlation function $G_d(r)$ for liquid propane at 92 K (top) and 228 K (bottom). The 228 K results have been displaced by 2 units along the vertical. Curves represent results from x-ray diffraction (Ref. 50) and the AIREBO model.

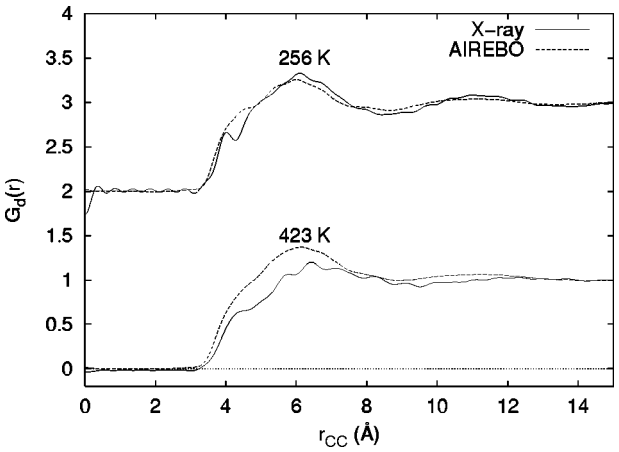

FIG. 6. Distinct intermolecular pair correlation function G_d for liquid neopentate at 256 K (top) and 423 K (bottom). The 423 K results have been displaced by 2 units along the vertical. Curves represent results from x-ray diffraction (Ref. 52) and the AIREBO model.

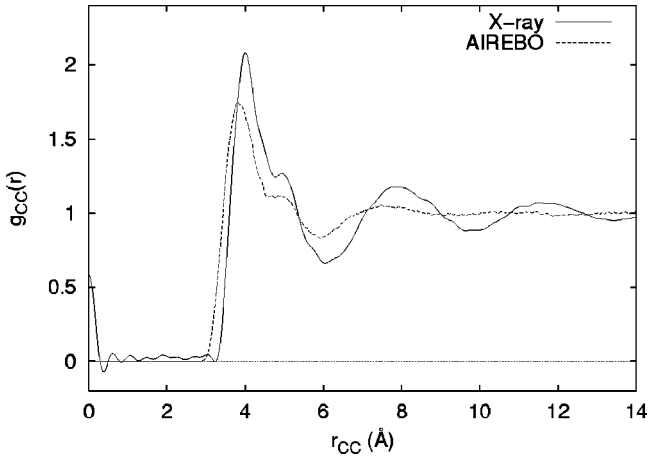

FIG. 7. Carbon–carbon pair correlation function g_{CC} for liquid ethylene at 106 K. Curves represent results from x-ray diffraction (Ref. 54) and the AIREBO model.

3.1 Å than is seen experimentally, indicating that extended *trans* form is sampled more frequently in the simulation than in experiment.

For neopentane (Fig. 6), the agreement is good at 256 K, and somewhat too structured at 423 K. The simulations do not reproduce the oscillatory nature of the experimental data, which may represent Fourier artifacts from the experimental data treatment. The peak near 4 Å is thought to be significant, however, and appears as a very weak shoulder in the simulation results.

Two unsaturated liquid hydrocarbons have been examined as well. Figure 7 shows the g_{CC} pair correlation functions for ethylene at 106 K that result from both simulation and experiment.[54] The simulated liquid here is less ordered than the real fluid, with little structure evident beyond the second solvation shell. The results for benzene (Fig. 8) are similar: accurate locations for the multiple peaks in the first-neighbor shell, but less structure than the experimental data[55] beyond the second shell.

Energetic properties of liquid hydrocarbons have been calculated also. The enthalpy of vaporization, $\Delta_{vap}H$, is calculated from the difference in internal energy for a single molecule in the gas and liquid phases at the specified temperature,

$$\Delta_{vap}H = E^{gas} - \frac{1}{N}E^{liq} + RT. \tag{19}$$

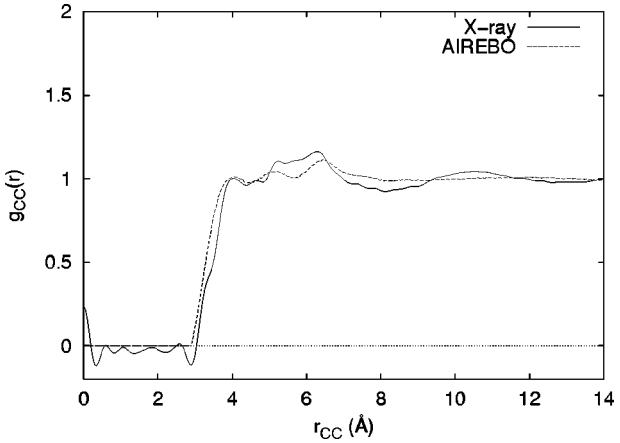

FIG. 8. Carbon–carbon pair correlation function g_{CC} for liquid benzene at 298 K. Curves represent results from x-ray diffraction (Ref. 55) and the AIREBO model.

TABLE V. Hydrocarbon properties. All $\Delta_{vap}H$ values correspond to the boiling point of the liquid.

Property	AIREBO	Expt.
Enthalpies of vaporization (kcal/mol):		
Methane (111.65 K)	2.3	2.0[a]
Ethane (184.55 K)	3.7	3.5[a]
Propane (231.05 K)	5.0	4.5[a]
Butane (272.65 K)	5.2	5.4[a]
Conformational energy differences (kcal/mol):		
Ethane $\Delta E^{\ddagger}$	2.9	2.9[b]
Propane $\Delta E^{\ddagger}$	3.4	3.4[c]
n-Butane ΔE (gauche-anti)	0.9	0.9[d]
n-Butane $\Delta E^{\ddagger}$ (synclinal-anti)	3.8	3.6[d]
n-Butane $\Delta E^{\ddagger}$ (syn-anti)	7.5	5.25[e]
2-Butene ΔE (cis-trans)	1.1	1.0[f]
2-Methylpropane $\Delta E^{\ddagger}$	3.9	3.9[g]
Methylcyclohexane ΔE (ax-eq)	2.0	1.75[h]
Bond enthalpies (kcal/mol):		
H—CH_3	110.0	104.8[i]
H—C_2H_5	98.0	100.3
H_3C—CH_3	93.0	89.8
H_2C=CH_2	172.0	172.0

[a]Reference 66.
[b]Reference 38.
[c]Reference 39.
[d]Reference 40.
[e]Reference 67.
[f]Reference 68.
[g]Reference 69.
[h]Cited in Ref. 70.
[i]Reference 58.

The enthalpies of vaporization of liquid methane and liquid ethane at their respective boiling points are reproduced satisfactorily (to within several tenths of a kcal/mol), because these properties were used explicitly in the fitting procedure. However, Table V demonstrates that the enthalpies of other hydrocarbon liquids are predicted equally well. Due to the lack of intermolecular interactions in the REBO potential, that model predicts liquid-state energies that are essentially no different from the gas-phase energies, giving $\Delta_{vap}H \approx RT$ for all molecular liquids.

The observed densities of several hydrocarbon liquids under 1 bar pressure are listed in Table VI. These include each of the liquids and state points examined in Figs. 2 through 7, including several liquids at more than one temperature. The average error in the density is 6.7%. This is reasonable, especially given that the current model makes use of only four LJ parameters to control intermolecular interactions. Density errors beneath 5% can be obtained by increasing the number of LJ parameters.[10,56,57] Errors as low as 1% can be achieved by force fields intended for use on specific sets of molecules, such as linear alkanes.[8,9] But the LJ parameters used in these models would not be expected to be transferable to other classes of hydrocarbons or carbon

TABLE VI. Liquid hydrocarbon densities, in g/cm^3.

Liquid	T(K)	AIREBO	Expt.[a]
Methane	92	0.477	0.453
Ethane	105	0.610	0.634
Ethane	181	0.518	0.554
Propane	92	0.685	0.725
Propane	228	0.539	0.586
Butane	140	0.692	0.726
Butane	267	0.548	0.606
Neopentane	256	0.601	0.633
Neopentane	423	0.322	0.364
Ethylene	106	0.631	0.655
Benzene	298	0.784	0.874

[a]Reference 58.

polytypes. Here we have aimed for a simple representation of the intermolecular interactions that gives reasonable results across a wide range of systems.

Gas-phase hydrocarbon molecules are also modeled more accurately than they are with the REBO potential, due to the presence of a dihedral-angle potential. The torsional barriers and conformer energy differences for several small molecules are listed in Table V. The 2.9 kcal/mol barrier to rotation in ethane[38] is fit accurately because it was used to determine the ϵ_{HCCH} parameter used in Eq. (13). Similarly, the 3.4 kcal/mol barrier in propane[39] and the 0.9 kcal/mol energy difference[40] between the *gauche* and *anti* forms of *n*-butane were used to determine ϵ_{CCCH} and ϵ_{CCCC}. The barrier heights in butane were not used in the fitting procedure, however, and are accurately reproduced.

Conformational energy differences are listed for several other hydrocarbons in Table V. These include energy differences in more congested single-bond rotations, ring substitutions, and geometric isomerism. In each of these cases, the agreement with experiment is within several tenths of a kcal/mol. While certainly not a complete survey of conformational energy differences, this sample suggests that the AIREBO model can be expected to provide reasonable descriptions of simple hydrocarbons.

As with diamond and graphite, the covalent bonding properties of the model remain largely unperturbed after the introduction of nonbonded interactions. The C–H bond dissociation enthalpy at 298 K is 110 kcal/mol in methane and 98 kcal/mol in ethane using the AIREBO model, compared to experimental values of 105 and 100 kcal/mol, respectively.[58] For C–C bonds, AIREBO predicts dissocation enthalpies of 93 kcal/mol in ethane and 172 kcal/mol in ethylene, compared to experimental values[58] of 90 and 172 kcal/mol. In each case, the AIREBO and REBO results differ from experiment by less than 5 kcal/mol.

V. DISCUSSION

The addition of torsion, dispersion, and nonbonded repulsion interactions to the REBO potential via an adaptive method has resulted in a new hydrocarbon potential that is suitable for studying reactivity in molecular condensed phases. The new potential overcomes the limitations of the REBO potential in studying systems with intermolecular interactions.

In particular, the new potential has been designed for molecular systems such as liquid hydrocarbons and thin films. Structural and energetic properties for a variety of small hydrocarbon molecules compare quite well with experiment. Further studies on self-assembled monolayers of hydrocarbon materials are also in progress, and are quite encouraging.[59,60]

The potential performs adequately on systems where the original REBO potential excelled. The density and elastic constants for diamond are off by several percent from the REBO potential, which is itself in good agreement with experiment. This indicates that there are systems, such as bulk diamond, for which REBO is still better suited. This is a result of the parametrization procedure, in which it was decided to leave as many REBO parameters as possible unaltered. Presumably a thorough reparametrization of the REBO portions of the potential would be able to correct these deficiencies, resulting in a single potential that is appropriate for modeling chemical reactions over the full range of carbon and hydrocarbon systems. Such a reparametrization could also address other issues with both the REBO and AIREBO potentials. Originally, the REBO bonding potential was kept very short-ranged to prevent covalent bonding interactions between nonneighboring atoms.[15] This resulted in an excessively short-ranged potential, particularly for interactions with surfaces.[28] While the introduction of LJ terms alleviates some aspects of this problem, the limited range of the covalent bonding potential has not been addressed here. Now that a mechanism is in place to handle nonbonded interactions, a reparametrization could include a lengthening of the covalent bonding portion of the REBO potential.

Another possible improvement involves an implementation of coordination-dependent LJ parameters. An implementation involving switching functions to smoothly vary the LJ parameters with bonding environment is fairly straightforward, but has not been attempted here.

The AIREBO potential is able to reproduce the structure of alkane liquids quite accurately, at a number of different state points. The agreement with experiment is generally quite good, although the high-temperature liquids are somewhat too structured. The performance on the two unsaturated hydrocarbons examined, while still reasonable, demonstrates a noticeable lack of long-range order when compared with experiment. This lack of long-ranged structure is quite possibly due to the complete lack of electrostatic interactions in the AIREBO model. These effects can often be ignored in saturated hydrocarbons, but unsaturated systems have nonnegligible bond dipoles and polarizabilities. The addition of these electrostatic effects to the AIREBO potential would clearly be useful, not only to improve the accuracy of the potential for unsaturated hydrocarbons, but also to enable reactive simulations of systems containing heteroatoms.

We have not undertaken a large-scale survey of hydrocarbon geometries and conformational energy differences, as existing molecular mechanics potentials undoubtedly do a better job of reproducing these properties for most mol-

ecules. The intent was to introduce a realistic, reactive potential that would be reasonably accurate for simple hydrocarbons. Modern molecular mechanics potentials, for example, are typically accurate to within thousandths of an angstrom in bond lengths, where the current potential is accurate only to hundredths of an angstrom. With only three parameters devoted to describing torsional interactions and four to the LJ interactions, rather than dozens of each in molecular mechanics force fields, the AIREBO model will most likely fail in some manner for many exotic hydrocarbons. Nonetheless, it performs reasonably over a fairly broad range of simple hydrocarbon species, and maintains as its principal advantage an ability to treat bond dissocation and formation.

Although the AIREBO potential has been developed for cases where reactivity is relevant, the results presented here have concentrated on the structural and energetic properties of a variety of systems. This is necessary to guarantee that the wide range of nonreactive properties typically required of a simulation potential are satisfied, in addition to the reactivity. While no dynamic properties have been considered here, these will be consequences of the potential energy surface predicted by the model. Furthermore, as indicated by the results above, the LJ and torsion interactions are only small perturbations on the unmodified covalent bonding portions of the potential, and alter their results only slightly. Thus, the bond energies and barriers presented in Tables III, IV and V, together with the prior successes of the predecessor REBO model,[15,17,20–27] provide some assurance that the model will provide for realistic bond dissociation and formation dynamics. Nonetheless, dynamic simulations involving bond dissociation and formation have not been presented here, and are left to future studies.

In summary, it is expected that the new AIREBO potential should prove to be a useful addition to the computational chemist's arsenal, complementary to both the original REBO and traditional molecular mechanics potentials. For carbon or hydrocarbon systems in which chemical reactions are of interest, and which require nonbonded interactions to be treated, the AIREBO potential provides an effective and accurate method of performing molecular simulations.

ACKNOWLEDGMENTS

This work was supported by the Office of Naval Research (#N00014-99-WR-20002) and the Air Force Office of Scientific Research (#NMIPR-99-5203042). We gratefully acknowledge Don Brenner for supplying the parameter values and computer program implementation of his REBO model prior to publication.

APPENDIX

The AIREBO potential can be represented by a sum over pairwise interactions, including covalent bonding (REBO) interactions, LJ terms, and torsion interactions:

$$E=\frac{1}{2}\sum_i\sum_{j\neq i}\left[E_{ij}^{\mathrm{REBO}}+E_{ij}^{\mathrm{LJ}}+\sum_{k\neq i,j}\sum_{l\neq i,j,k}E_{kijl}^{\mathrm{tors}}\right]. \tag{A1}$$

The REBO interaction is based on the form proposed by Tersoff,[1]

$$E_{ij}^{\mathrm{REBO}}=V_{ij}^{\mathrm{R}}+b_{ij}V_{ij}^{\mathrm{A}}, \tag{A2}$$

in which repulsive and attractive contributions are combined in a ratio determined by the bonding term b_{ij}.

The repulsive term has the form used by Brenner,[18]

$$V_{ij}^{\mathrm{R}}=w_{ij}(r_{ij})\left[1+\frac{Q_{ij}}{r_{ij}}\right]A_{ij}e^{-\alpha_{ij}r_{ij}}, \tag{A3}$$

where the parameters Q_{ij}, A_{ij}, and α_{ij} depend on the atom types i and j. Values for these and all other potential parameters are given in Table II. The w_{ij} term is a bond-weighting factor,

$$w_{ij}(r_{ij})=S'(t_c(r_{ij})), \tag{A4}$$

that switches off the REBO interactions when the atom pairs exceed typical bonding distances. The switching function takes the form

$$S'(t)=\Theta(-t)+\Theta(t)\Theta(1-t)\tfrac{1}{2}[1+\cos(\pi t)], \tag{A5}$$

where the switching region for each type of bond is given by a scaling function,

$$t_c(r_{ij})=\frac{r_{ij}-r_{ij}^{\min}}{r_{ij}^{\max}-r_{ij}^{\min}}. \tag{A6}$$

The attractive pair interaction in Eq. (A2) is given by a triple exponential,

$$V_{ij}^{\mathrm{A}}=-w_{ij}(r_{ij})\sum_{n=1}^{3}B_{ij}^{(n)}e^{-\beta_{ij}^{(n)}r_{ij}}, \tag{A7}$$

which is switched off smoothly for nonshort-ranged interactions through the use of the bond weight.

The b_{ij} term in Eq. (A2) specifies the ''bond order'' for the interaction between atoms i and j,

$$b_{ij}=\tfrac{1}{2}[p_{ij}^{\sigma\pi}+p_{ji}^{\sigma\pi}]+\pi_{ij}^{\mathrm{rc}}+\pi_{ij}^{\mathrm{dh}}. \tag{A8}$$

This term is only roughly equivalent to the usual chemical concept of a bond order, and is simply a means of modifying the strength of a bond due to changes in the local environment. The b_{ij} term is larger for stronger bonds.

Each of the terms that contribute to b_{ij} is a many-body term that depends on the bonding environment surrounding atoms i and j. The principal contribution to b_{ij} is the covalent bond interaction, given by the terms $p_{ij}^{\sigma\pi}$ and $p_{ji}^{\sigma\pi}$.

$$p_{ij}^{\sigma\pi}=\left[1+\sum_{k\neq i,j}w_{ik}(r_{ik})g_i(\cos\theta_{jik})e^{\lambda_{jik}}+P_{ij}\right]^{-1/2}. \tag{A9}$$

Note that $p_{ij}^{\sigma\pi}$ is not necessarily equal to $p_{ji}^{\sigma\pi}$. The $p_{ij}^{\sigma\pi}$ term depends on the bond angles θ_{jik} between the $\mathbf{r}_{ji}$ vector and the vectors $\mathbf{r}_{ki}$ to any other neighboring atoms.

The penalty function g_i imposes a cost on bonds that are too close to one another. Its functional form is a fifth-order spline. When the central atom is a carbon, the spline also depends on the local coordination number, defined as the sum of the carbon-only and hydrogen-only coordination numbers,

TABLE VII. Interpolation points for the quintic spline $g_i(\cos\theta)$ [cf. Eqs. (A9) and (A12)].

	$\cos\theta$	g_i	$\partial g_i/\partial(\cos\theta)$	$\partial^2 g_i/\partial(\cos\theta)^2$
$g_C^{(1)}$:	-1	$-0.010\,000$	0.104 000	0.000 000
[Eq. (A12)]	$-\frac{2}{3}$	0.028 207	0.131 443	0.140 229
	$-\frac{1}{2}$	0.052 804	0.170 000	0.370 000
	$-\frac{1}{3}$	0.097 321	0.400 000	1.98 000
	1	1.00 000	2.834 57	10.2647
$g_C^{(2)}$:	-1	$-0.0100\,00$	0.104 000	0.000 000
[Eq. (A12)]	$-\frac{2}{3}$	0.028 207	0.131 443	0.140 229
	$-\frac{1}{2}$	0.052 804	0.170 000	0.370 000
	$-\frac{1}{3}$	0.097 321	0.400 000	1.980 00
	1	8.000 00	20.2436	43.9336
g_H:	-1	11.2357	0.000 000	115.115
[Eq. (A9)]	$-\frac{5}{6}$	12.5953	13.8543	32.3618
	$-\frac{1}{2}$	16.8111	8.641 23	-25.0617
	1	19.9918	0.333 013	$-0.474\,189$

TABLE VIII. Interpolation points for the bicubic spline $P_{ij}(N_i^C, N_i^H)$ [cf. Eq. (A9)]. All values not listed, and all derivatives, are zero at integral values of N_i^C and N_i^H.

	N_{ij}^C	N_{ij}^H	P_{ij}
$P_{CC}(N_{ij}^C, N_{ij}^H)$:			
	0	2	$-0.000\,500$
	0	3	0.016 125
	1	1	$-0.010\,960$
	1	2	0.006 326
	2	0	$-0.027\,603$
	2	1	0.003 180
$P_{CH}(N_{ij}^C, N_{ij}^H)$:			
	0	1	0.209 337
	0	2	$-0.064\,450$
	0	3	$-0.303\,928$
	1	0	0.010 000
	1	1	$-0.125\,123$
	1	2	$-0.298\,905$
	2	0	$-0.122\,042$
	2	1	$-0.300\,529$
	3	0	$-0.307\,585$

$$N_{ij} = N_{ij}^C + N_{ij}^H, \tag{A10}$$

where

$$N_{ij}^C = \left(\sum_{k \neq i} \delta_{kC} w_{ik}(r_{ik}) \right) - \delta_{jC} w_{ij}(r_{ij}), \tag{A11}$$

counts a carbon-only coordination number, with δ_{ij} representing a Kronecker delta. The hydrogen-only coordination number N_{ij}^H is defined similarly. (Note that the coordination number of atom i, in the context of the $i-j$ bond, is defined so as to exclude the neighbor j from the count.) Using this coordination number, the angle-bending penalty function g_i switches smoothly between a form $g_C^{(1)}$ appropriate for covalent compounds with low coordination and another form $g_C^{(2)}$ suitable for highly coordinated bulk materials,

$$g_C(\cos\theta_{jik}) = g_C^{(1)}(\cos\theta_{jik}) + S'(t_N(N_{ij}))[g_C^{(2)}(\cos\theta_{jik}) - g_C^{(1)}(\cos\theta_{jik})]. \tag{A12}$$

At intermediate values of N, the switching function $S'(t_N)$ provides for a smooth transition, with S' given by Eq. (A5), and the scaling function t_N given by

$$t_N(N_{ij}) = \frac{N_{ij} - N_{ij}^{\min}}{N_{ij}^{\max} - N_{ij}^{\min}}. \tag{A13}$$

The coefficients of the g_i fifth-order splines are determined by the values of the function and its first two derivatives specified at the interpolation points listed in Table VII.

The two remaining terms in Eq. (A9) are small correction factors. The $e^{\lambda_{jik}}$ term is added to improve the potential energy surface for abstraction of hydrogen atoms from hydrocarbons, with

$$\lambda_{jik} = 4\delta_{iH}[(\delta_{kH}\rho_{HH} + \delta_{kC}\rho_{CH} - r_{ik}) - (\delta_{jH}\rho_{HH} + \delta_{jC}\rho_{CH} - r_{ij})], \tag{A14}$$

where δ_{ij} represents the Kronecker delta for atom types i and j.

The P_{ij} term is a two-dimensional cubic spline[61] in N_{ij}^C and N_{ij}^H, whose coefficients are chosen to reproduce the values of P_{ij} and its derivatives at the interpolation points listed in Table VIII. These terms are included in the REBO model to give accurate bond energies for small hydrocarbons. Although most REBO parameters were not modified in developing the AIREBO model, the P_{ij} values were modified at two points to counteract the additional torsion energies in the AIREBO potential for unsaturated systems such as ethylene and graphite.

In addition to the covalent bonding interactions given by Eq. (A9), the REBO potential also includes contributions to the bond order from radical and conjugation effects. These enter the potential through the π_{ij}^{rc} term, which is a three-dimensional cubic spline[61] in the variables N_{ij}, N_{ji}, and N_{ij}^{conj}. The indices N_{ij} and N_{ji} are the coordination numbers defined in Eq. (A10), and N_{ij}^{conj} is a local measure of conjugation in the $i-j$ bond,

$$N_{ij}^{conj} = 1 + \left[\sum_{k \neq i,j} \delta_{kC} w_{ik}(r_{ik}) S'(t_{conj}(N_{ki})) \right]^2 + \left[\sum_{l \neq i,j} \delta_{lC} w_{jl}(r_{jl}) S'(t_{conj}(N_{lj})) \right]^2, \tag{A15}$$

with t_{conj} specifying the range of coordination numbers under which a bond is assumed to be part of a radical or conjugated network:

$$t_{conj}(N) = \frac{N - N^{\min}}{N^{\max} - N^{\min}}. \tag{A16}$$

The N_{ij}^{conj} variable, which is unity for nonconjugated bonds and can be as high as nine in polyaromatic compounds, is an empirical measure of unsaturation that is based entirely on coordination. The interpolation points for the three-dimensional spline π_{ij}^{rc} are provided in Table IX.

TABLE IX. Interpolation points for tricubic spline $\pi_{ij}^{\mathrm{rc}}(N_{ij},N_{ji},N^{\mathrm{conj}})$ [cf. Eq. (A8)]. The function is symmetric, so $\pi_{ji}^{\mathrm{rc}}(N_{ji},N_{ij},N^{\mathrm{conj}})=\pi_{ij}^{\mathrm{rc}}(N_{ij},N_{ji},N^{\mathrm{conj}})$. Only one of each symmetric pair of interpolation values is listed. All other values and derivatives not listed are zero at integral values of N_{ij}, N_{ji}, and $N^{\mathrm{conj}_{ij}}$.

	N_{ij}	N_{ji}	N_{ij}^{conj}	π_{ij}^{rc}	$\partial\pi_{ij}^{\mathrm{rc}}/\partial N_{ij}$	$\partial\pi_{ij}^{\mathrm{rc}}/\partial N_{ji}$	$\partial\pi_{ij}^{\mathrm{rc}}/\partial N^{\mathrm{conj}}$
$\pi_{\mathrm{CC}}^{\mathrm{rc}}$:							
	0	0	$\geqslant 3$	0.004 959	0	0	0
	1	0	1	0.021 694	0	0	0
	1	0	$\geqslant 2$	0.004 959	0	0	0
	1	1	1	0.052 500	0	0	0
	1	1	2	−0.002 089	0	0	0
	1	1	$\geqslant 3$	−0.008 043	0	0	0
	2	0	1	0.024 699	0	0	0
	2	0	2	−0.005 971	0	0	0
	2	0	$\geqslant 3$	0.004 959	0	0	0
	2	1	1	0.004 825	−0.026 250	0	0
	2	1	2	0.015 000	0	0	0
	2	1	3	−0.010 000	0	0	0
	2	1	4	−0.011 689	0	0	−0.010 022
	2	1	5	−0.013 378	−0.027 188	0	−0.010 022
	2	1	6	−0.015 067	−0.027 188	0	0
	2	1	$\geqslant 7$	−0.015 067	−0.027 188	0	0
	2	2	1	0.047 225	0	0	0
	2	2	2	0.011 000	0	0	0
	2	2	3	0.019 853	0	0	0
	2	2	4	0.016 544	0	0	−0.003 309
	2	2	5	0.013 235	0	0	−0.003 309
	2	2	6	0.009 926	0	0	−0.003 309
	2	2	7	0.006 618	0	0	−0.003 309
	2	2	8	0.003 309	0	0	−0.003 309
	3	0	1	−0.099 899	0	0	0
	3	0	2	−0.099 899	0	0	0
	3	0	$\geqslant 3$	0.004 959	0	0	0
	3	1	2	−0.062 418	0	0.037 545	0
	3	1	$\geqslant 3$	−0.062 418	0	0	0
	3	2	1	−0.022 355	0	0	0
	3	2	$\geqslant 2$	−0.022 355	0	0.062 418	0
$\pi_{\mathrm{CH}}^{\mathrm{rc}}$:							
	1	1	1	−0.050 000	0	0	0
	1	1	2	−0.050 000	0	0	0
	1	1	3	−0.300 000	0	0	0
	1	1	$\geqslant 4$	−0.050 000	0	0	0
	2	0	$\geqslant 5$	−0.004 524	0	0	0
	2	1	2	−0.250 000	0	0	0
	2	1	3	−0.250 000	0	0	0
	3	1	1	−0.100 000	0	0	0
	3	1	2	−0.125 000	0	0	0
	3	1	3	−0.125 000	0	0	0
	3	1	$\geqslant 4$	−0.100 000	0	0	0
$\pi_{\mathrm{HH}}^{\mathrm{rc}}$:							
	1	1	1	0.124 916	0	0	0

The remaining contribution to the bond order b_{ij} is π_{ij}^{dh}. This term imposes a penalty for rotation around multiple bonds,

$$\pi_{ij}^{\mathrm{dh}}=T_{ij}(N_{ij},N_{ji},N_{ij}^{\mathrm{conj}})\sum_{k\neq i,j}\sum_{l\neq i,j}(1-\cos^2\omega_{kijl})\times w'_{ik}(r_{ik})w'_{jl}(r_{jl})\Theta(\sin(\theta_{jik})-s^{\min})\times\Theta(\sin(\theta_{ijl})-s^{\min}). \tag{A17}$$

Here T_{ij} is another three-dimensional cubic spline, with interpolation points given in Table X. The torsion angle ω_{kijl} is defined in the usual way as the angle between the plane defined by the vectors $\mathbf{r}_{ik}$ and $\mathbf{r}_{ij}$ and that defined by $\mathbf{r}_{ij}$ and $\mathbf{r}_{jl}$,

TABLE X. Interpolation points for the tricubic spline $T_{ij}(N_{ij},N_{ji},N^{\mathrm{conj}})$ [cf. Eq. (A17)]. Values not listed, and all derivatives, are zero at integral values of N_{ij}, N_{ji}, and N_{ij}^{conj}.

N_{ij}	N_{ji}	N_{ij}^{conj}	T_{ij}
2	2	1	−0.035 140
2	2	$\geqslant 2$	−0.004 048

$$\cos\omega_{kijl}=\frac{\mathbf{r}_{ji}\times\mathbf{r}_{ik}}{|\mathbf{r}_{ji}\times\mathbf{r}_{ik}|}\cdot\frac{\mathbf{r}_{ij}\times\mathbf{r}_{jl}}{|\mathbf{r}_{ij}\times\mathbf{r}_{jl}|}. \tag{A18}$$

The bond-weighting function

$$w'_{ij}(r_{ij})=S'(t'_c(r_{ij})), \tag{A19}$$

used in Eq. (A17) differs slightly from that defined in Eq. (A4), through a different scaling function t'_c:

$$t'_c(r_{ij})=\frac{r_{ij}-r_{ij}^{\min}}{r_{ij}^{\max'}-r_{ij}^{\min}}. \tag{A20}$$

The LJ and torsional contributions to the energy are described in detail in the text. However, for completeness, the equations and parameters are reproduced here. The LJ contribution to the $i-j$ pair energy,

$$E_{ij}^{\mathrm{LJ}}=S(t_r(r_{ij}))S(t_b(b_{ij}^{*}))C_{ij}V_{ij}^{\mathrm{LJ}}(r_{ij}) +[1-S(t_r(r_{ij}))]C_{ij}V_{ij}^{\mathrm{LJ}}(r_{ij}), \tag{A21}$$

includes the traditional LJ term

$$V_{ij}^{\mathrm{LJ}}(r_{ij})=4\epsilon_{ij}\left[\left(\frac{\sigma_{ij}}{r_{ij}}\right)^{12}-\left(\frac{\sigma_{ij}}{r_{ij}}\right)^{6}\right], \tag{A22}$$

modified by several sets of switching functions. The switching function $S(t)$ differs in form from that of Eq. (A5),

$$S(t)=\Theta(-t)+\Theta(t)\Theta(1-t)[1-t^2(3-2t)]. \tag{A23}$$

Both have continuous first derivatives at the switching region boundaries.

Below a certain separation $r_{ij}^{\mathrm{LJ\,max}}$, the magnitude of the LJ term depends on the bonding environment. The gradual exclusion of LJ interactions as r_{ij} changes is controlled by the t_r scaling function,

$$t_r(r_{ij})=\frac{r_{ij}-r_{ij}^{\mathrm{LJ\,min}}}{r_{ij}^{\mathrm{LJ\,max}}-r_{ij}^{\mathrm{LJ\,min}}}. \tag{A24}$$

At intramolecular distances, the LJ interaction is included only if there is no significant bonding interaction between the two atoms, as specified by the t_b switch,

$$t_b(b_{ij})=\frac{b_{ij}-b_{ij}^{\min}}{b_{ij}^{\max}-b_{ij}^{\min}}, \tag{A25}$$

and if the atoms i and j are not connected by two or fewer intermediate atoms. This latter switch is controlled by bond weights,

$$C_{ij}=1-\max\{w_{ij}(r_{ij}),\ w_{ik}(r_{ik})w_{kj}(r_{kj}),\quad \forall k\ w_{ik}(r_{ik})w_{kl}(r_{kl})w_{lj}(r_{lj}),\forall k,l\}. \tag{A26}$$

The torsional potential for the dihedral angle determined by atoms i, j, k, and l is controlled by the term

$$E_{kijl}^{\mathrm{tors}}=w_{ki}(r_{ki})w_{ij}(r_{ij})w_{jl}(r_{jl})V^{\mathrm{tors}}(\omega_{kijl}), \tag{A27}$$

where

$$V^{\mathrm{tors}}(\omega_{kijl})=\frac{256}{405}\epsilon_{kijl}\cos^{10}(\omega_{kijl}/2)-\frac{1}{10}\epsilon_{kijl}. \tag{A28}$$

[1] J. Tersoff, Phys. Rev. B **37**, 6991 (1988).
[2] J. Tersoff, Phys. Rev. B **39**, 5566 (1989).
[3] W. L. Jorgensen, J. D. Madura, and C. J. Swenson, J. Am. Chem. Soc. **106**, 6638 (1984).
[4] N. L. Allinger, K. Chen, and J.-H. Lii, J. Comput. Chem. **17**, 642 (1996).
[5] W. L. Jorgensen, D. S. Maxwell, and J. Tirado-Rives, J. Am. Chem. Soc. **118**, 11225 (1996).
[6] W. D. Cornell, P. Cieplak, C. Bayly, I. R. Gould, K. M. Merz, D. M. Ferguson, D. C. Spellmeyer, T. Fox, J. W. Caldwell, and P. A. Kollman, J. Am. Chem. Soc. **117**, 5179 (1995).
[7] T. A. Halgren, J. Comput. Chem. **17**, 490 (1996).
[8] S. K. Nath, F. A. Escobedo, and J. J. de Pablo, J. Chem. Phys. **108**, 9905 (1998).
[9] M. G. Martin and J. I. Siepmann, J. Phys. Chem. B **102**, 2569 (1998).
[10] H. Sun, J. Phys. Chem. B **102**, 7338 (1998).
[11] J. Tersoff, Phys. Rev. Lett. **61**, 2879 (1988).
[12] D. W. Brenner, Mater. Res. Soc. Symp. Proc. **141**, 59 (1989).
[13] M. V. R. Murty and H. A. Atwater, Phys. Rev. B **51**, 4889 (1995).
[14] A. J. Dyson and P. V. Smith, Surf. Sci. **355**, 140 (1996).
[15] D. W. Brenner, Phys. Rev. B **42**, 9458 (1990).
[16] D. W. Brenner, Phys. Rev. B **46**, 1948 (1992).
[17] D. W. Brenner, J. A. Harrison, C. T. White, and R. J. Colton, Thin Solid Films **206**, 220 (1991).
[18] D. W. Brenner, S. B. Sinnott, and J. A. Harrison (unpublished).
[19] J. A. Harrison, S. J. Stuart, D. H. Robertson, and C. T. White, J. Phys. Chem. B **101**, 9682 (1997).
[20] S. B. Sinnott, R. J. Colton, C. T. White, O. A. Shendeova, D. W. Brenner, and J. A. Harrison, J. Vac. Sci. Technol. A **15**, 936 (1997).
[21] J. A. Harrison, C. T. White, R. J. Colton, and D. W. Brenner, Phys. Rev. B **46**, 9700 (1992).
[22] J. A. Harrison, R. J. Colton, C. T. White, and D. W. Brenner, Wear **168**, 127 (1993).
[23] J. A. Harrison, C. T. White, R. J. Colton, and D. W. Brenner, J. Phys. Chem. **97**, 6573 (1993).
[24] J. A. Harrison and D. W. Brenner, J. Am. Chem. Soc. **116**, 10399 (1994).
[25] J. A. Harrison, C. T. White, R. J. Colton, and D. W. Brenner, Thin Solid Films **260**, 205 (1995).
[26] M. D. Perry and J. A. Harrison, Langmuir **12**, 4552 (1996).
[27] J. A. Harrison, S. J. Stuart, and D. W. Brenner, in *Handbook of Micro/Nano Tribology*, 2nd ed., edited by B. Bhushan (CRC, New York, 1999).
[28] P. de Sainte Claire, K. Song, W. L. Hase, and D. W. Brenner, J. Chem. Phys. **100**, 1761 (1996).
[29] R. Smith and K. Beardmore, Thin Solid Films **272**, 255 (1996).
[30] M. R. Nyden, T. R. Coley, and S. Mumby, Polym. Eng. Sci. **37**, 1496 (1997).
[31] J. Che, T. Çağin, and W. A. Goddard III, Theor. Chem. Acc. **102**, 346 (1999).
[32] S. J. Stuart and B. J. Berne, J. Phys. Chem. **100**, 11934 (1996).
[33] M. D. Perry and J. A. Harrison, J. Phys. Chem. B **101**, 1364 (1997).
[34] A. Warshel and S. Lifson, J. Chem. Phys. **53**, 582 (1970).
[35] W. L. Jorgensen, J. Phys. Chem. **87**, 5304 (1983).
[36] E. Burgos, E. Halac, and H. Bonadeo, Chem. Phys. Lett. **298**, 273 (1998).
[37] G. H. Hudson and J. C. McCoubrey, Trans. Faraday Soc. **56**, 761 (1959).
[38] E. Hirota, Y. Endo, S. Saito, and J. L. Duncan, J. Mol. Spectrosc. **89**, 285 (1981).
[39] J. P. Lowe, Prog. Phys. Org. Chem. **6**, 1 (1968).
[40] D. A. C. Compton, S. Montero, and W. F. Murphy, J. Phys. Chem. **84**, 3587 (1980).
[41] J. C. Boettger, Phys. Rev. B **55**, 11202 (1997).
[42] A. Fukumoto, Phys. Rev. B **42**, 7462 (1990).
[43] J. Bernholc, A. Antonelli, T. M. Del Sole, Y. Bar-Yam, and S. T. Pantelides, Phys. Rev. Lett. **61**, 2689 (1988).
[44] E. Kaxiras and K. C. Pandey, Phys. Rev. Lett. **61**, 2693 (1988).
[45] M. P. Allen and D. J. Tildesley, *Computer Simulation of Liquids* (Oxford University Press, London, 1987).
[46] S. A. Adelman and J. D. Doll, J. Chem. Phys. **64**, 2375 (1976).
[47] H. J. C. Berendsen, J. P. M. Postma, W. F. van Gunsteren, A. Di Nola, and J. R. Haak, J. Chem. Phys. **81**, 3684 (1984).
[48] A. Habenschuss, E. Johnson, and A. H. Narten, J. Chem. Phys. **74**, 5234 (1981).
[49] S. I. Sandler, M. G. Lombardo, D. S.-M. Wong, A. Habenschuss, and A. H. Narten, Chem. Phys. **77**, 2144 (1982).
[50] A. Habenschuss and A. H. Narten, J. Chem. Phys. **85**, 6022 (1986).

[51] A. Habenschuss and A. H. Narten, J. Chem. Phys. **91**, 4299 (1989).
[52] A. H. Narten, J. Chem. Phys. **70**, 299 (1979).
[53] A. Habenschuss (private communication).
[54] A. H. Narten and A. Habenschuss, J. Phys. Chem. **75**, 3073 (1981).
[55] A. H. Narten, J. Chem. Phys. **67**, 2102 (1977).
[56] G. Kaminski, E. M. Duffy, T. Matsui, and W. L. Jorgensen, J. Phys. Chem. **98**, 13077 (1994).
[57] J. Nagy, D. F. Weaver, and V. H. Smith, Jr., J. Phys. Chem. **99**, 8058 (1995).
[58] *CRC Handbook of Chemistry and Physics*, edited by D. R. Lide (Chemical Rubber, Boca Raton, 1990).
[59] A. B. Tutein, S. J. Stuart, and J. A. Harrison, J. Phys. Chem. B **103**, 11357 (1999).
[60] A. B. Tutein, S. J. Stuart, and J. A. Harrison, Langmuir **16**, 291 (2000).
[61] W. H. Press, B. P. Flannery, S. A. Teukolsky, and W. T. Vetterling, *Numerical Recipes* (Cambridge University Press, Cambridge, 1986).
[62] N. N. Greenwood and A. Earnshaw, *Chemistry of the Elements* (Pergamon, New York, 1984).
[63] H. J. McSkimin and P. Andreatch, Jr., J. Appl. Phys. **43**, 2944 (1972).
[64] *Handbook of Carbon, Graphite, Diamond and Fullerenes*, edited by H. O. Pierson (Noyes Publications, Park Ridge, New Jersey, 1993).
[65] O. L. Blakslee, D. G. Proctor, E. J. Seldin, G. B. Spence, and T. Weng, J. Appl. Phys. **41**, 3373 (1970).
[66] F. D. Rossini, K. S. Pitzer, R. L. Arnett, R. M. Braun, and G. C. Pimentel, *Selected Values of Physical and Thermodynamic Properties of Hydrocarbons and Related Compounds* (Carnegie, Pittsburgh, 1953).
[67] N. L. Allinger, R. S. Grev, B. F. Yates, and H. F. Schaefer III, J. Am. Chem. Soc. **112**, 114 (1990).
[68] N. L. Allinger, F. Li, and L. Yan, J. Comput. Chem. **11**, 848 (1990).
[69] D. R. Lide, Jr. and D. E. Mann, J. Chem. Phys. **29**, 914 (1958).
[70] K. Gundertofte, J. Palm, I. Petterson, and A. Stamvik, J. Comput. Chem. **11**, 200 (1991)